Miner Petrol (2018) 112:245–256
DOI 10.1007/s00710-017-0531-1

ORIGINAL PAPER

Raman spectroscopic features of Al- Fe^{3+}- poor magnesiochromite and Fe^{2+}- Fe^{3+}- rich ferrian chromite solid solutions

Sherif Kharbish[1]

Received: 11 May 2017 / Accepted: 22 August 2017 /Published online: 29 August 2017

Abstract Naturally occurring Al- Fe^{3+}- poor magnesiochromite and Fe^{2+}- Fe^{3+}- rich ferrian chromite solid solutions have been analyzed by micro-Raman spectroscopy. The results reflect a strong positive correlation between the Fe^{3+} # [Fe^{3+}/(Fe^{3+}+Cr + Al)] and the positions of all Raman bands. A positive correlation of the Raman band positions with Mg# [Mg/(Mg + Fe^{2+})] is less stringent. Raman spectra of magnesiochromite and ferrian chromite show seven and six bands, respectively, in the spectral region of 800 − 100 cm^{-1}. The most intense band in both minerals is identified as symmetric stretching vibrational mode, $\nu_1(A_{1g})$. In the intermediate Raman-shift region (400–600 cm^{-1}), the significant bands are attributed to the $\nu_3(F_{2g}) > \nu_4(F_{2g}) > \nu_2(E_g)$ modes. The bands with the lowest Raman shifts (< 200 cm^{-1}) are assigned to F_{2g}(*trans*) translatory lattice modes. Extra bands in magnesiochromite (two bands) and in ferrian chromite (one weak band) are attributed to lowering in local symmetry and order/disorder effects.

Keywords Raman spectroscopy · Magnesiochromite · Ferrian chromite · Spinel · Ferritchromite · Order–disorder

Introduction

Micro-Raman spectroscopy provides facts on the structure and chemistry of numerous mineral groups (e.g. Beran and Libowitzky 2004; Smith and Dent 2005; Dubessy et al. 2012) and facilitates an exact, conspicuous determination of major minerals (e.g., silicates; Wang et al. 1999; Dubessy et al. 2012), accessory minerals (e.g., phosphates, oxides and sulfides; Kharbish 2012; White 2009; Kharbish et al. 2014), and secondary minerals (e.g., sulfates, carbonates, sulfosalts and phyllosilicate clay minerals; Wang et al. 2002a; White 2009; Kharbish and Andráš 2014; Kharbish and Jeleň 2016; Kharbish 2016, 2017). It can also identify the hydroxyl group and the bound and unbound types of water (Libowitzky 1999; Wang et al. 2001; Dubessy et al. 2012).

Spinel group minerals belong to a large group of oxides (in a closer sense and in contrast to sulfide spinels) with the general chemical formula $A^{2+}B^{3+}{}_2O_4$ (A = Mg, Fe^{2+}, etc., B = Cr, Al, Fe^{3+}, etc.). They crystallize in the cubic space group *Fd3m*, with an almost cubic close packing of oxygen anions, and with A and B cations at interstitial tetrahedral (T) and octahedral (M) sites (D'lppolito et al. 2015). In general, A^{2+} and B^{3+} cations can occupy on both T and M sites, thus resulting in a variable degree of disorder, which is expressed by the inversion parameter i (defined as the fraction of the B^{3+} cations at the T sites; Sickafus et al. 1999). In the spinel minerals, two ordered configurations occur at low and ambient temperatures, i.e. the normal spinel structure $^{T}A^{M}B_2X_4$ with $i = 0$ and the completely inverse spinel structure $^{T}B^{M}(AB)X_4$ with $i = 1$ (D'lppolito et al. 2015).

Chromium bearing spinels (Cr-spinel) are the most important ore minerals of the metal chromium and are common raw materials for refractory industry. Among them, Mg-rich Cr-spinel (magnesiochromite, $MgCr_2O_4$) is very sensitive to conditions during rock formation; therefore, it stores information concerning the tectonic settings in which its host rocks crystallized. Thus Mg-rich Cr-spinel is vastly considered a significant petrogenetic indicator (e.g. Barnes 2000; Kharbish 2013). Fe^{2+}- Fe^{3+}-rich Cr-spinel (ferrian

Editorial handling: L. Nasdala

✉ Sherif Kharbish
sherif.abdalla@suezuniv.edu.eg;
sherifkharbish@hotmail.com

[1] Geology Department, Faculty of Science, Suez Governorate, Suez University, El Salam City 43518, Egypt

chromite; $(Fe^{2+},Mg)(Cr,Fe^{3+})_2O_4$; informally referred to as ferritchromite) is considered as an alteration product of Cr-spinel (e.g. Barnes 2000).

Most previous Raman investigations have focused on the Raman-active mode assignments and the spectral features of natural and synthetic spinels with different compositions (e.g. Malézieux et al. 1983; Malézieux 1985; Wang et al. 2002b; Yong et al. 2012; Lenaz and Lughi 2013; D'lppolito et al. 2015). Only a few articles dealt with the change in the Raman spectra within a solid solution series (Reddy and Frost 2005; Lenaz and Lughi 2013, 2017; Lenaz and Skogby 2013; Wang et al. 2002b; Yong et al. 2012).

Except for the Raman studies of synthetic series $MgCr_2O_4$ – $MgFe_2O_4$ by Lenaz and Lughi (2013) and natural Al-rich Cr-spinel (Lenaz and Lughi 2017), no Raman spectroscopic studies to the best of the author's knowledge, have characterized naturally occurring Al^{3+}- Fe^{3+}- poor magnesiochromite and Fe^{2+}- Fe^{3+}- rich ferrian chromite solid solutions. Considering the importance of these solid solutions as petrographic indicators for the host rock genesis and alteration conditions, the present article aims, therefore, at a systematic analysis of the characteristic Raman spectroscopic features of the naturally occurring magnesiochromite and ferrian chromite solid solutions and to specify the chemical substitution effects on their Raman spectra.

Samples and experiments

Samples used in the present work are from different localities in the central Eastern Desert of Egypt (e.g. Gabal Al-Degheimi, Kab Amiri district and Gabal El-Rubshi). These localities belong to the Arabian–Nubian Shield (ANS) that covers huge areas of NE Africa and the Arabian Peninsula and are covered by a dismembered ophiolite of Precambrian age, where their ultramafic section is well-developed, being dominated by serpentinites (Kharbish 2010, 2013). Stratigraphically, the Neoproterozoic ANS comprises four units; volcanosedimentary successions, dismembered ophiolite complexes, gabbro–diorite-tonalite complexes and unmetamorphosed volcanic and pyroclastic sequences that are intruded by granodiorite–granite complexes (Kharbish 2010, 2013). Spinels are hosted in serpentinites and occur interstitially as isotropic irregular zoned fractured grains of gray color and red internal reflection (visual appearance of polished sections under a reflected light microscope). The core of the grain that is identified as magnesiochromite, is darker than the outer rim (identified as ferrian chromite) which is lighter gray in color due to higher reflectance.

A Cameca electron probe microanalyzer (EPMA; Cameca SX 100, 15 kV accelerating voltage, 20 nA beam current, 1 µm beam diameter) was used to determine their chemical compositions. The peak and background counting times were 10 and 5 s, respectively. The investigated minerals were analyzed using the K_α line for Si, Al, Cr, Fe, Mg, Mn, Ca and Ti. Data were calibrated by natural and synthetic reference materials (adularia for Si, Al; chromite for Cr, Fe; periclase for Mg; rhodonite for Mn; wollastonite for Ca and rutile for Ti) and were corrected by the ZAF software.

The charge balance equation of Droop (1987) was used to calculate Fe^{3+} from EPMA data. In general, the number of Fe^{3+} ions per X oxygens in the mineral formula, F, is given by; $F = 2 \times (1 - T/S)$, where T is the ideal number of cations per formula unit, and S is the observed cation total per X (= 32) oxygens calculated assuming all iron to be Fe^{2+}.

The non-polarized micro-Raman spectra were acquired on a Horiba JobinYvon LabRAM-HR, in the spectral range from 50 to 1200 cm^{-1}. 632.8 nm excitation from a He-Ne laser with a polarization extinction exceeding 500: 1 was focused with a 100×/0.80 objective on the sample surface. To avoid heating influence on samples, the incident laser was attenuated to < 1 mW energy (measured behind the objective). The spectra were collected in quasi-backscatter geometry and analyzed with a 1200 lines/mm grating monochromator. The spectral resolution and wavenumber accuracy were 0.8 cm^{-1} in the red range and ± 2 cm^{-1}, respectively. Data acquisition, instrument control, baseline correction and background subtraction were performed with LabSpec 5 software (Horiba Jobin–Yvon). Based on the signal intensity, eight acquisitions with 60–90 s per 'spectral window' were adopted. Accurate band centers were determined by band fitting assuming combined Gaussian–Lorentzian (Voigt) band shapes, using the PeakFit 4.12 software (Jandel Scientific).

Results and discussion

Mineral chemistry

The investigated magnesiochromites (Fig. 1) are Al-Fe^{3+}-poor Cr-spinels having a high Cr# [= Cr/(Cr + Al + Fe^{3+}); 0.63–0.75], a low Fe^{3+}# [= Fe^{3+}/ (Fe^{3+}+Cr + Al); < 0.10] and Al_2O_3 content (9.84–18.06 wt%) (Table 1). They are chemically characterized by an intermediate Mg# [=Mg/(Mg + Fe^{2+}); 0.43–0.57] (Table 1). The studied magnesiochromites show the following approximate compositions: $(Mg_{0.43-0.57},Fe^{2+}_{0.42-0.57})(Al_{0.38-0.68},Cr_{1.26-1.50},Fe^{3+}_{0.02-0.16})O_4$.

The composition of ferrian chromite (Fig. 1) is characterized by very small amounts of Al_2O_3 (< 1 wt%), similar Cr_2O_3 (~ 20–39 wt%) and FeO contents (~ 25–30 wt%) and higher Fe_2O_3 contents (~ 27–48 wt%). Therefore, they are characterized by a high Fe^{3+}# (0.46–0.70), a high Fe^{2+}# [Fe^{2+}/(Mg + Fe^{2+}); 0.80–0.94] and thus Mg # (0.06–0.20) (Table 1). The studied ferrian chromites show

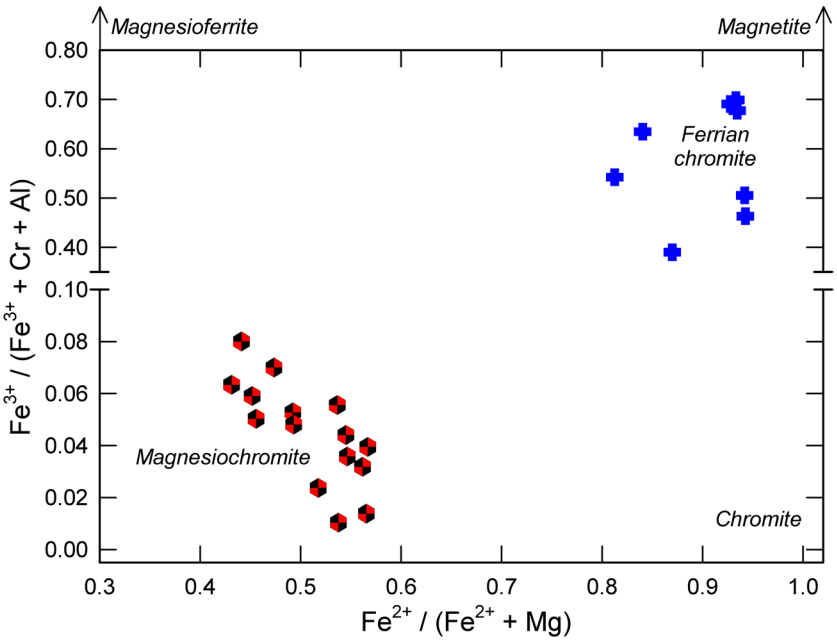

Fig. 1 Plot of Fe^{3+}# against Fe^{2+}# (i.e. the fraction of Fe^{3+} in three-valent cations against the fraction of Fe^{2+} in two-valent cations; in apfu; data from Table 1), visualizing the chemical compositions of the spinels investigated. Sizes of symbols exceed the analytical errors

the approximate compositions $(Mg_{0.06-0.19},Fe^{2+}{}_{0.78-0.94})(Al_{0.00-0.04},Cr_{0.61-1.16},Fe^{3+}{}_{0.78-1.36})O_4$.

Raman spectroscopy

Factor group analysis and band assignment

Magnesiochromite and ferrian chromite Raman spectra are depicted in Fig. 2, a band summary is given in Table 2. In the cubic spinel structure (space group *Fd3m*, No. 227; O_h point symmetry, $Z=8$) the O anionic array is described by the Wyckoff position 32(e) [$3m$ (C_{3v}) site symmetry]. The A^{2+} and B^{+3} atoms occupy only 1/8 of all potential T sites [8(a) Wyckoff position, $-43m$ (T_d)] and 1/2 of all potential M sites [16(d), $-3m$ (D_{3d})]. The number of Raman- and infrared- (IR) active phonons is evaluated for a definite crystal structure via group theory in the form of classical factor group analysis (FGA) using the O_h spectroscopic symmetry. The F-centered unit cell of the investigated minerals contains 56 atoms (i.e. 8 A^{2+}, 16 B^{3+}, 32 O), however, the primitive (Bravais) unit cell contains 14 atoms leading to 42° of freedom (39 vibrations corresponding to optical modes and three modes to acoustic vibrations) as predicted by FGA. In terms of irreducible representations (Γ), these 42 normal vibrational modes at the Brillouin zone center can be decomposed as:

$$\Gamma = A_{1g}(R) + 2A_{2u} + E_g(R) + 2E_u + F_{1g} + 5F_{1u}(IR) + 3F_{2g}(R) + 2F_{2u},$$

The (R) and (IR) identify Raman- and IR-active modes, respectively, whereas the rest of the species are silent or acoustic modes. The E and F modes are doubly and triply degenerate, respectively and the three acoustic modes belong to one F_{1u} species. Thus, FGA predicts five and four active optical modes in Raman- (i.e. $A_{1g}+E_g+3F_{2g}$) and IR- (viz. $4F_{1u}$) spectroscopy, respectively.

Band assignments for the investigated minerals are based on the sequence of band energies given in the literature (e.g. Chopelas and Hofmeister 1991; Wang et al. 2002b, 2004; Reddy and Frost 2005; Laguna-Bercero et al. 2007; Errandonea 2014; D'lppolito et al. 2015): $\nu_1(A_{1g}) > \nu_3(F_{2g}) > \nu_4(F_{2g}) > \nu_2(E_g) > F_{2g}(trans)$ [*trans* = translatory lattice mode]. In the present work, the internal vibration of the $^{M}BO_6$ octahedron is considered to be the major contributor to the main Raman bands of the investigated minerals based on the following reasons.

The covalency degrees of B^{3+}- O bonds (41–49%) in spinels are high relative to those of A^{2+} - O bonds (31% and 29%) (Wang et al. 2001). The degree of covalency of a chemical bond in a crystal structure is generally applied to predict the major ionic group contributing to Raman spectral features (Chopelas and Hofmeister 1991; Wang et al. 2001). The ^{M}B – O central interatomic force constant dominates over the ^{T}A – O one for the Raman- and IR-active vibrations (Gupta et al. 1989). Moreover, Laguna-Bercero et al. (2007) mentioned that the higher-energy vibrations in spinels depend more strongly on the nature of the octahedral cation.

The high-Raman-shift bands located between 690 and 710 cm^{-1} in magnesiochromite and between 670 and

Table 1 Representative results of EPMA chemical analyses and calculated mineral formulae for magnesiochromite and ferrian chromite

Mineral	Magnesiochromite											
Constituent	MC1	MC2	MC3	MC4	MC5	MC6	MC7	MC8	MC9	MC10	MC11	MC12
EPMA results (wt%)												
SiO_2	0.56	0.03	0.00	0.00	0.11	0.42	1.15	0.35	0.14	0.35	0.01	0.11
TiO_2	0.09	0.08	0.10	0.00	0.00	0.00	0.00	0.00	0.08	0.06	0.07	0.05
Al_2O_3	12.47	13.58	16.58	9.92	11.74	12.27	13.85	12.54	12.26	9.84	11.74	18.06
Cr_2O_3	52.65	55.98	49.87	56.39	56.81	53.69	50.69	53.88	55.16	55.45	55.69	49.51
Fe_2O_3	4.17	0.84	4.15	4.40	1.09	4.74	3.08	3.85	2.53	5.55	2.85	1.95
FeO	17.72	19.61	16.84	18.82	20.16	16.30	20.88	18.08	20.28	16.69	19.22	18.84
MnO	0.95	0.37	0.51	0.77	0.46	1.29	1.21	0.44	0.44	1.54	0.69	1.15
MgO	10.25	9.46	11.28	9.12	8.69	11.09	8.95	10.42	8.88	10.41	8.95	9.85
CaO	0.25	0.00	0.03	0.00	0.00	0.00	0.00	0.00	0.00	0.00	0.04	0.00
Total	99.10	99.95	99.37	99.42	99.06	99.81	99.81	99.55	99.77	99.89	99.64	99.51
Calculated mineral formulae (apfu)[a]												
Si	0.02	0.00	0.00	0.00	0.00	0.01	0.04	0.01	0.00	0.01	0.00	0.00
Ti	0.00	0.00	0.00	0.00	0.00	0.00	0.00	0.00	0.00	0.00	0.00	0.00
Al	0.48	0.52	0.63	0.39	0.46	0.47	0.54	0.48	0.48	0.38	0.46	0.68
Cr	1.37	1.45	1.27	1.50	1.50	1.38	1.31	1.40	1.44	1.45	1.46	1.26
Fe^{3+}	0.10	0.02	0.10	0.11	0.03	0.12	0.08	0.10	0.06	0.14	0.07	0.05
Fe^{2+}	0.49	0.54	0.45	0.53	0.56	0.44	0.57	0.50	0.56	0.46	0.53	0.51
Mn	0.02	0.00	0.01	0.02	0.01	0.03	0.03	0.01	0.01	0.04	0.01	0.03
Mg	0.50	0.46	0.54	0.46	0.43	0.54	0.44	0.51	0.44	0.51	0.44	0.47
Ca	0.01	0.00	0.00	0.00	0.00	0.00	0.00	0.00	0.00	0.00	0.00	0.00
Mg#[b]	0.51	0.46	0.54	0.46	0.43	0.55	0.43	0.51	0.44	0.53	0.45	0.48
Cr#[b]	0.70	0.73	0.63	0.75	0.75	0.70	0.68	0.71	0.73	0.74	0.73	0.63
Fe^{3+}#[b]	0.052	0.010	0.050	0.056	0.014	0.059	0.040	0.048	0.031	0.070	0.036	0.024
Mineral	Magnesiochromite				Ferrian chromite							
Constituent	MC13	MC14	MC15		MF1	MF2	MF3	MF4	MF5	MF6	MF7	MF8
EPMA results (wt%)												
SiO_2	0.03	0.12	0.23		0.42	1.05	0.19	0.56	0.42	0.35	0.00	0.33
TiO_2	0.08	0.00	0.01		0.25	0.29	0.31	0.29	0.22	0.44	0.40	0.00
Al_2O_3	15.41	11.01	14.05		0.83	0.20	0.19	0.00	0.81	0.19	1.01	0.97
Cr_2O_3	50.53	55.76	49.85		31.17	20.40	28.95	19.55	34.21	23.96	29.40	39.43
Fe_2O_3	5.22	3.49	6.47		34.76	45.57	40.07	47.65	32.08	44.20	38.44	27.84
FeO	15.94	19.23	15.42		29.80	27.99	25.15	27.39	30.19	26.41	25.67	28.16
MnO	0.51	0.54	1.51		0.66	3.17	1.32	3.17	0.68	1.42	1.14	0.76
MgO	11.79	9.00	10.95		1.03	1.10	3.52	1.10	1.03	2.81	3.32	2.17
CaO	0.03	0.11	0.02		0.19	0.19	0.17	0.05	0.00	0.17	0.00	0.00
Total	99.55	99.53	99.25		99.11	99.95	99.88	99.75	99.64	99.94	99.38	99.65
Calculated mineral formulae (apfu)[a]												
Si	0.00	0.00	0.01		0.02	0.04	0.01	0.02	0.02	0.01	0.00	0.01
Ti	0.00	0.00	0.00		0.01	0.01	0.01	0.01	0.01	0.01	0.01	0.00
Al	0.58	0.43	0.54		0.04	0.01	0.01	0.00	0.04	0.01	0.04	0.04
Cr	1.28	1.47	1.29		0.93	0.61	0.85	0.58	1.01	0.70	0.86	1.16
Fe^{3+}	0.13	0.09	0.16		0.99	1.29	1.11	1.36	0.91	1.24	1.07	0.78
Fe^{2+}	0.43	0.54	0.42		0.94	0.88	0.78	0.87	0.95	0.82	0.80	0.87
Mn	0.01	0.01	0.04		0.02	0.10	0.04	0.10	0.02	0.04	0.03	0.02
Mg	0.57	0.45	0.53		0.06	0.06	0.19	0.06	0.06	0.16	0.18	0.12
Ca	0.00	0.00	0.00		0.01	0.01	0.01	0.00	0.00	0.01	0.00	0.00
Mg#[b]	0.57	0.45	0.56		0.06	0.07	0.20	0.07	0.06	0.16	0.19	0.12
Cr#[b]	0.64	0.74	0.65		0.48	0.32	0.43	0.30	0.52	0.36	0.44	0.59
Fe^{3+}#[b]	0.063	0.044	0.080		0.50	0.68	0.57	0.70	0.46	0.63	0.54	0.39

[a]Calculated based on 32 oxygen atoms per formula unit

[b]$Mg\# = Mg/(Mg + Fe^{2+})$, $Cr\# = Cr/(Cr + Al + Fe^{3+})$, $Fe^{3+}\# = Fe^{3+}/(Fe^{3++}Cr + Al)$

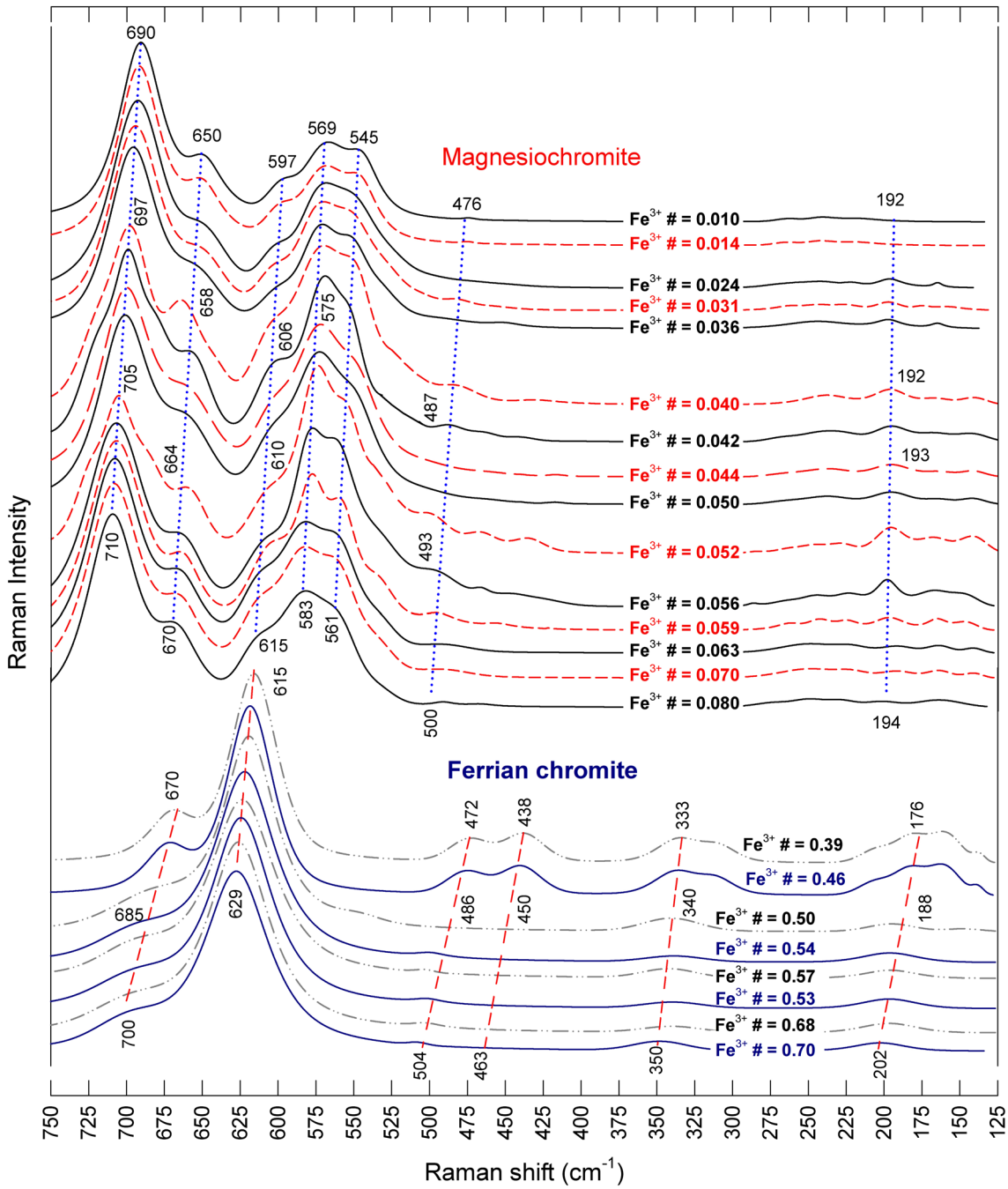

Fig. 2 Raman spectra of magnesiochromite and ferrian chromite solid solutions. Raman-shift values of the main bands (obtained by band fitting; goodness of fit $r^2 > 0.997$) are quoted

700 cm^{-1} in ferrian chromite (Table 2 and Fig. 2) are viewed as the $v_1(A_{1g})$ symmetric stretching vibration of the $^{M}BO_6$ groups (B=Cr, Al, Fe^{3+}). The medium to weak intensity bands in the intermediate Raman-shift region in magnesiochromite (597–615 cm^{-1}, Table 2 and Fig. 2) and ferrian chromite (615–629 cm^{-1}, Table 2 and Fig. 2), are attributed to the $v_3(F_{2g})$ modes in agreement with previous studies (e.g. Lenaz and Lughi 2013, 2017; D'lppolito et al. 2015). This mode has been also assigned to the $^{M}BO_6$ groups symmetric stretching vibration (Reddy and Frost 2005; Marinković Stanojević et al. 2007).

The assignments of the E_g and $v_4(F_{2g})$ species are quite controversial. While Wang et al. (2002b) and Zhang and Gan (2011) assigned the bands around 500 cm^{-1} to E_g symmetry and those around 450 cm^{-1} to $v_4(F_{2g})$ symmetry, others, did it in the opposite way (e.g. Sinha 1999; Lenaz and

Table 2 Spectral positions and assignment for Raman bands of magnesiochromite and ferrian chromite, in comparison with literature data

Mineral	Fe^{3+}#	Assignment							
		$v_1(A_{1g})$		$v_3(F_{2g})$		$v_4(F_{2g})$	$v_2(E_g)$		F_{2g} (trans)
Magnesiochromite	0.010	690	650	597	569	545	476		192
	0.014	691	651	598	570	546	478		193
	0.024	692	653	599	570	548	480		193
	0.031	694	655	600	571	549	481		192
	0.036	695	656	601	572	550	482		192
	0.040	697	658	603	573	550	485		192
	0.042	699	659	606	574	552	487		194
	0.044	700	660	607	575	553	489		193
	0.050	701	661	608	576	554	490		194
	0.052	705	664	610	578	555	491		194
	0.056	706	665	611	578	557	493		193
	0.059	707	667	612	579	559	495		192
	0.063	708	668	613	580	560	497		193
	0.070	709	669	614	581	560	499		194
	0.080	710	670	615	583	561	500		194
Ferrian chromite	0.39	670		615		472	438	333	176
	0.46	675		618		479	442	336	180
	0.50	681		620		486	450	340	188
	0.54	685		621		490	454	342	192
	0.57	689		623		494	457	343	194
	0.63	694		625		497	459	348	197
	0.68	698		627		500	462	349	200
	0.70	700		629		504	463	350	202
Wang et al. (2002b) $MgCr_2O_4$		687		614		544	447		227
Wang et al. (2004) $FeCr_2O_4$		690		650		600	445		
Reddy and Frost (2005) $FeCr_2O_4$		730				560	445		
Yong et al. (2012) $MgCr_2O_4$		684		613		543	447		
D'Ippolito et al. (2015) $MgCr_2O_4$		684		612		542	446		

All Raman-shift values are quoted in cm^{-1}

Lughi 2013; D'lppolito et al. 2015). Based on the commonly accepted sequence of modes (see above) and theoretical calculations by Sinha (1999) to predict the zone center phonon frequencies for spinels, the bands at 545–561 cm^{-1} (magnesiochromite, Table 2 and Fig. 2) and at 472 to 504 cm^{-1} (ferrian chromite, Table 2 and Fig. 2) correspond to the $v_4(F_{2g})$ bending vibrations (Marinković Stanojević et al. 2007). The E_g symmetric ^{M}B–O stretching vibrations (Reddy and Frost 2005; Marinković Stanojević et al. 2007) occur from 476 to 500 cm^{-1} (magnesiochromite, Table 2 and Fig. 2) and from 438 to 463 cm^{-1} (ferrian chromite, Table 2 and Fig. 2).

The lowest and weakest Raman shift F_{2g}(*trans*) band was considered as a translatory lattice mode (Marinković Stanojević et al. 2007; Errandonea 2014; D'lppolito et al. 2015). In the present study the F_{2g}(*trans*) lattice vibrations appear around 195 cm^{-1} in both magnesiochromite and ferrian chromite (Table 2 and Fig. 2).

In addition to the above described modes, two weak bands and shoulders occur from 650 to 670 and from 569 to 583 cm^{-1} (Table 2 and Fig. 2) in magnesiochromite and one weak band appears from 333 to 350 cm^{-1} (Table 2 and Fig. 2) in ferrian chromite. Similar unexpected modes were recorded by many other authors (e.g. Wang et al. 2002a, b, 2004; Marinković Stanojević et al. 2007; D'lppolito et al. 2015), while their origin remained unclear.

Band positions and numbers

Figure 2 reveals that all Raman bands of magnesiochromite and ferrian chromite increase in Raman shift (blue shift) and additionally change in band shape and amplitude with increasing Fe^{3+} #. In addition, the Raman spectra of the studied minerals show more bands (7 in magnesiochromite and 6 in ferrian chromite) than predicted by FGA (Fig. 2).

Except for the A_{1g} mode, the blue shifts of other Raman bands (i.e. to higher Raman-shift values) with increasing Fe^{3+} # are inconsistent with what has been published so far (e.g. Wang et al. 2002a, 2004; Lenaz and Lughi 2013, 2017;

D'lppolito et al. 2015). In fact, higher Raman shifts that are observed for all bands with increasing content of the heavier Fe^{3+} ions and elongated/weakened bonds (relative to Cr), are an unexpected feature. This observation is in stark contrast to the general physics of vibrational spectroscopy and to previously published literature (e.g. D'lppolito et al. 2015; Lenaz and Lughi 2013, 2017).

The band position can be calculated by Hooke's law: $v = 1/2\pi\sqrt{f/u}$ derived by the model of the harmonic oscillator, in which f is the force constant which characterizes bond stiffness, and u is the reduced mass (defined by $u = m_A . m_B / m_A + m_B$). The mass difference between Fe and Cr ions is very small and consequently they have a very close reduced mass ($u_{Fe-O} = 20.65 \times 10^{-27}$ kg; $u_{Cr-O} = 20.31 \times 10^{-27}$ kg). Therefore their reduced masses have little or no effect on the vibration spectra. Preudhomme and Tarte (1971) mentioned that in spinels, the band positions depend mainly on the bonding force between the trivalent cation and the oxygen anion, with no significant relationship with the mass of the trivalent cations. Furthermore, Shannon's ionic radii (Shannon 1976) of B^{3+} are Fe > Cr > Al, therefore the B^{3+} - O bond distances are Fe > Cr > Al. Thus, the blue shifts of all Raman bands with increasing Fe^{3+} # cannot be attributed directly to the stronger bonds (i.e. higher force constant).

A possible explanation of this unexpected behavior is the inversion of the spinel structure. A temperature dependence study on cation inversion of magnesium ferrite ($MgFe_2O_4$) shows slight decrease in lattice parameter with increasing degree of inversion and is generally to be expected for 2–3 spinels, with cations of sizes similar to Mg^{2+} and Fe^{3+} (O'Neill et al. 1992). The cation inversion between the octahedral and tetrahedral sites forces the incorporated Fe^{3+} to occupy the tetrahedral site and thus the divalent cation occupies the octahedral sites (for more details see Sickafus et al. 1999). The inversion starts with initial substitution of iron, which is supported by theoretical calculations and experimental data. Park and Kim (1992) calculated the cation distribution of $NiFe_xCr_{2-x}O_4$ solid solution, and showed that at an iron content of $0 \le x \le 1$, nearly all the Ni^{2+} had been displaced from the tetrahedral sites. The same conclusion was reached by Allen et al. (1988) in their characterization for numerous Ni- Cr- Fe spinels. An increase in the inversion parameter as the Fe^{3+} content increases results in a decrease in the lattice parameter that could be attributed to the tetrahedrally coordinated Fe^{3+} having a smaller ionic radius than Mg^{2+} (Shannon 1976). The high-pressure studies on various spinels (e.g. Wang et al. 2002a, b) indicate an increase in Raman shift of the Raman-active modes with a decrease in unit cell volume of the spinels. From this contraction, affecting also the coordination octahedra at the M sites, it should be expected that the Raman-shift values of the samples investigated will increase significantly with increasing Fe^{3+} #.

It is worth mentioning that the change in unit cell volume could not be checked in the present work (e.g. by X-ray powder diffraction), because micro-analyses by EPMA data and Raman spectroscopy were acquired from single grains in a solid rock sample. Therefore, the question of whether the change in Raman-active modes due to the change in unit cell volume only, or other factors (e.g. changes in the high-spin / low-spin state of Fe^{3+}) could be the main contributors to the large changes in Raman-band positions, is not conclusively resolved.

The excess in the band number in the Raman spectrum of spinels was considered to be caused by lowering of the local crystal structure symmetry or was related to cation disorder (Chopelas and Hofmeister 1991; Cynn et al. 1992; Wang et al. 2002b; Van Minh and Yang 2004). It is generally accepted that the presence of vacancies, interstitial cations, nonstoichiometry and defects may result in additional modes not predicted by FGA. The local distortions around the B^{3+} cations may cause a reduced $^{M}BO_6$ octahedron symmetry from D_{3d} to C_{3v} and a crystal structure change from O_h to T_d, which increases the total number of Raman- (and IR-) active modes from five to seven (Grimes and Collett 1971). No apparent crystal symmetry degradation or structural modification was noticed, except for a regular shift to higher Raman-shift values with increasing Fe^{3+} #. Due to the lack of structure refinements, especially for ferrian chromite, a conclusive explanation of the appearance of extra modes in the investigated minerals due to lowering in the symmetry cannot be given. However, no apparent lowering in the spinel crystal symmetry was detected due to chemical substitution (Wang et al. 2004) or before and after annealing at high temperature (Van Minh and Yang 2004).

The appearance of the modes at 650–670 and 569–583 cm^{-1} (Fig. 2 and Table 2) in magnesiochromite and at 333 to 350 cm^{-1} (Fig. 2 and Table 2) in ferrian chromite can be directly related to the order–disorder effect of the A^{2+} and B^{3+} atoms over the T and M sites. The first-principles calculation by Lazzeri and Thilbaudeau (2006) proposed that the additional modes in spinel are related to an order–disorder transition and not to the presence of chemical impurities or to a combination of harmonic modes.

The $B^{3+}O_6$ group is a regular octahedron only for an ideal O positional parameter geometry ($u = 0.25$). Published structural data yield $u = \sim 0.262$ for magnesiochromite (e.g. O'Neill and Dollase 1994; Lenaz and Princivalle 2005) and $u = \sim 0.256$ for ferrian chromite (O'Neill et al. 1992). Furthermore, u is negatively correlated with the degree of order (Redfern et al. 1999). A distortion to a non-cubic $B^{3+}O_6$ group permits additional Raman bands by lifting of degeneracies or by releasing selection rules of certain modes inactive to active. The former observation may also explain the presence of two extra modes in the magnesiochromite

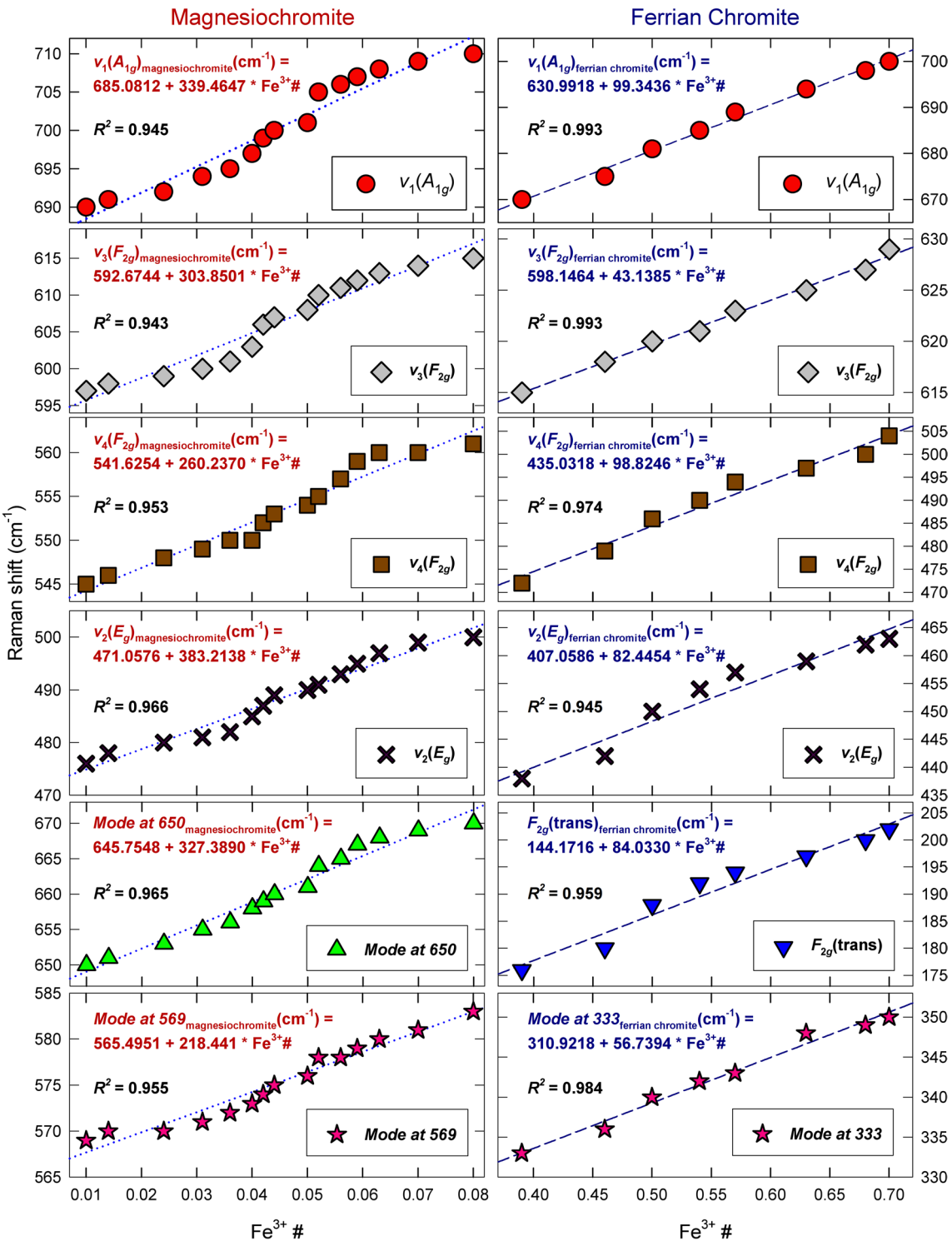

Fig. 3 Plots of Fe^{3+}# against Raman-band positions of magnesiochromite and ferrian chromite, visualizing positive correlations (correlation coefficients R^2 are quoted). Dotted and dashed lines are visual guides

($u > 0.262$) versus one additional mode in the ferrian chromite ($u > 0.256$).

The observation of DeAngelis et al. (1971) and Keramidas et al. (1975) that the completely ordered spinels (viz. normal spinels) exhibit a larger number of Raman and IR bands than the apparent disordered material (namely inverse spinels), explains the increase in band number, in general and the appearance of two additional bands in

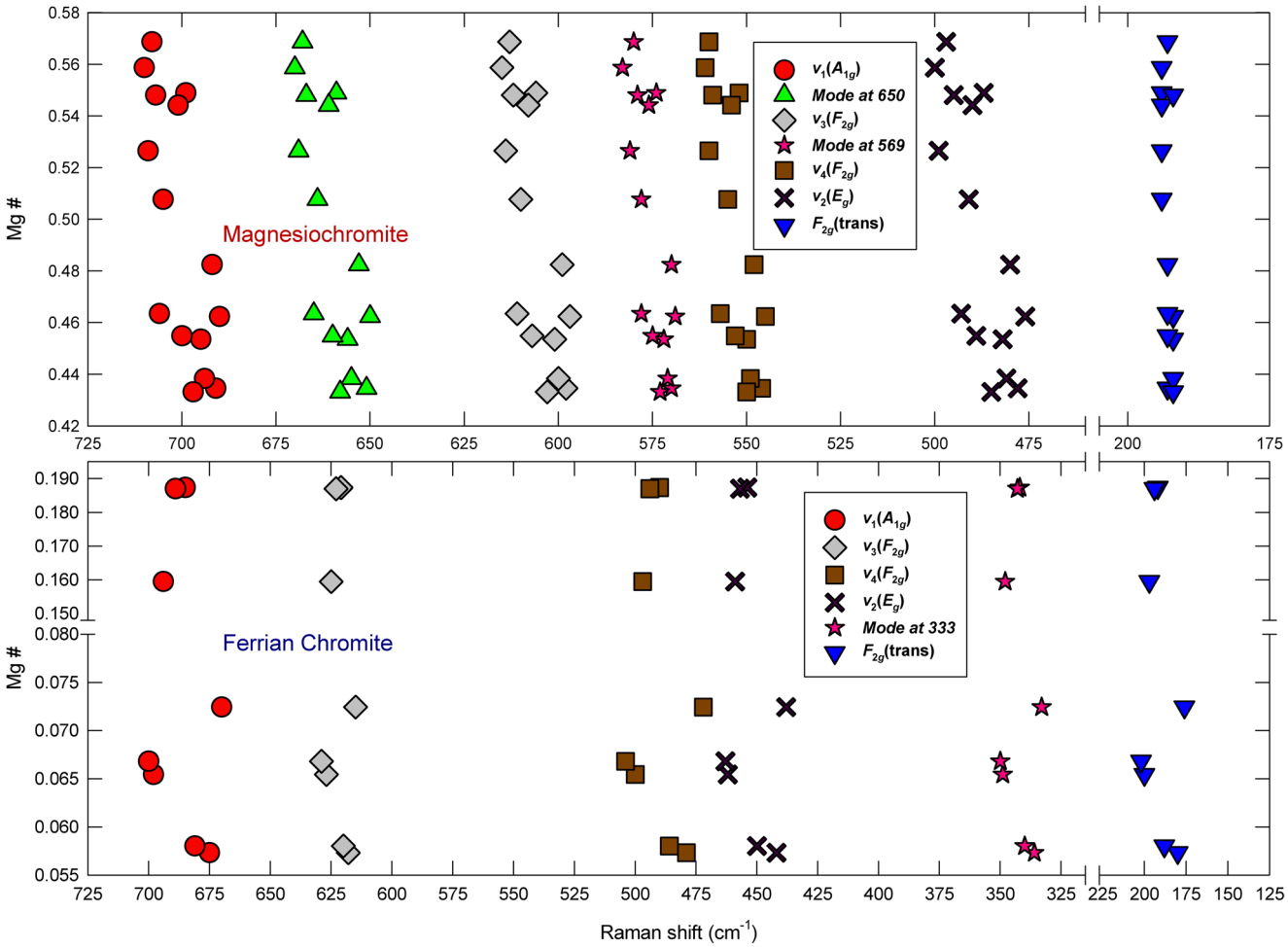

Fig. 4 Plot of Mg# against Raman-band positions of magnesiochromite and ferrian chromite

magnesiochromite (almost ordered state) in comparison with only one extra mode in the ferrian chromite (nearly disordered). It is clear also that the intensities of the extra mode in the ferrian chromite (Fig. 2) decrease with the increase of the Fe^{3+}# (i.e. toward the disordered direction).

Raman bands – spinel chemistry relations

The relation between the $\nu_1(A_{1g})$ Raman-band position and the chemical composition of natural and synthetic spinels was previously studied by different authors. Malézieux et al. (1983) and Wang et al. (2004) concluded that the position of the $\nu_1(A_{1g})$ mode in natural and synthetic spinels is the most useful for discriminating B^{3+} substitutions in the ulvöspinel-chromite and chromite-spinel solid-solutions. Moreover, the E_g band position can be used to discriminate between chromates (~450 cm^{-1}) and ferrites (~300 cm^{-1}) (D'lppolito et al. 2015).

The positive correlations of the band positions in magnesiochromite and ferrian chromite with Fe^{3+}# are shown in Fig. 3. Except for the $F_{2g}(trans)$ mode in magnesiochromites (not shown in Fig. 3) all modes show very high correlation coefficients between their positions and Fe^{3+}# (Fig. 3). Based on these correlations, it is obvious that not only the position of the $\nu_1(A_{1g})$ mode is useful for discriminating trivalent substitutions in spinels (according to Malézieux et al. 1983; Malézieux 1985; Wang et al. 2004), but also the other bands as well. It is probably not possible to determine whether the investigated natural spinels are chromate or ferrite spinels using the weak E_g mode as proposed by D'Ippolito et al. (2015). This is due to the fact that the investigated spinels do not show a clear E_g mode in the position suggested by D'Ippolito et al. (2015). However, the modes at ~650 and at ~550 cm^{-1} can be considered characteristic features for identifying at least chromate spinels.

Furthermore, the correlations can be employed to determine the band positions and / or the Fe^{3+}#. To simplify the diagrams of determining the band positions and / or the Fe^{3+}#, it is recommended to use the linear equations of the first-order polynomial fit obtained in Fig. 3. Therefore, for

the band positions and / or the Fe^{3+}# the equations are as follows:

$$\nu_1(A_{1g})_{magnesiochromite}(cm^{-1}) = 685.08 + 339.46 * Fe^{3+}\# \quad (1)$$

$$\nu_3(F_{2g})_{magnesiochromite}(cm^{-1}) = 592.67 + 303.85 * Fe^{3+}\# \quad (2)$$

$$\nu_4(F_{2g})_{magnesiochromite}(cm^{-1}) = 541.63 + 260.24 * Fe^{3+}\# \quad (3)$$

$$\nu_2(E_g)_{magnesiochromite}(cm^{-1}) = 471.06 + 383.21 * Fe^{3+}\# \quad (4)$$

$$Mode\ at\ 650_{magnesiochromite}(cm^{-1}) = 645.75 + 327.39 * Fe^{3+}\# \quad (5)$$

$$Mode\ at\ 569_{magnesiochromite}(cm^{-1}) = 565.50 + 218.44 * Fe^{3+}\# \quad (6)$$

$$\nu_1(A_{1g})_{ferrian\ chromite}(cm^{-1}) = 630.99 + 99.34 * Fe^{3+}\# \quad (7)$$

$$\nu_3(F_{2g})_{ferrian\ chromite}(cm^{-1}) = 598.15 + 43.14 * Fe^{3+}\# \quad (8)$$

$$\nu_4(F_{2g})_{ferrian\ chromite}(cm^{-1}) = 435.03 + 98.82 * Fe^{3+}\# \quad (9)$$

$$\nu_2(E_g)_{ferrian\ chromite}(cm^{-1}) = 407.06 + 82.45 * Fe^{3+}\# \quad (10)$$

$$F_{2g}(trans)_{ferrian\ chromite}(cm^{-1}) = 144.17 + 84.03 * Fe^{3+}\# \quad (11)$$

$$Mode\ at\ 333_{ferrian\ chromite}(cm^{-1}) = 310.92 + 56.74 * Fe^{3+}\# \quad (12)$$

Finally, a rather poor correlation was found between the observed band positions and Mg# indicating the A^{2+} substitutions in T sites of these samples (Fig. 4). This observation confirms the predominant effect of the B^{3+} substitutions in the M site on the Raman spectra. Lenaz and Lughi (2017) noticed also a poor relation between Mg# and the A_{1g} in natural Cr-spinels whereas Wang et al. (2004) observed no relation between the A_{1g} band position and $Fe^{2+}/(Fe^{2+}+Mg)$ in tetrahedral sites.

Conclusions

Raman spectroscopic investigations on magnesiochromite and ferrian chromite solid solutions yield Raman fingerprint spectra that can be utilized to gain information about their chemistry. From the above discussion and observations, it is suggested that (1) Raman spectra of magnesiochromite and ferrian chromite are dominated by vibrations of $^{M}BO_6$ groups rather than by $^{T}AO_4$ units; (2) all modes in the magnesiochromite and ferrian chromite spectra are mainly affected by the trivalent substitutions in M sites and are useful for estimating Fe^{3+} #; (3) the substitutions among divalent atoms (A^{2+}) in the T sites affect the band positions only weakly and (4) the order–disorder effect of the A^{2+} and B^{3+} atoms over the T and M sites causes the appearance of extra modes in the investigated minerals. The obtained results are without doubt interesting for gemology, mineralogy, geology and material sciences and a starting point for further investigations.

Acknowledgements Thanks are due to Eugen Libowitzky and three anonymous reviewers for their valuable comments that helped to improve the manuscript, and to journal editor Lutz Nasdala for his kind help.

References

Allen GC, Jutson JA, Tempest PA (1988) Characterization of nickel-chromium-iron spinel type oxides. J Nucl Mater 158:96–107. https://doi.org/10.1016/0022-3115(88)90159-6

Barnes SJ (2000) Chromite in komatiites II. Modification during green-schist to mid-amphibolite facies metamorphism. J Petrol 41:387–409. https://doi.org/10.1093/petrology/41.3.387

Beran A, Libowitzky E (2004) Spectroscopic methods in mineralogy. EMU notes om mineralogy 6. https://doi.org/10.1180/EMU-notes.6

Chopelas A, Hofmeister AM (1991) Vibrational spectroscopy of aluminate spinels at 1 atm and of $MgAl_2O_4$ to over 200 kbar. Phys Chem Miner 18:279–293. https://doi.org/10.1007/BF00200186

Cynn H, Sharma SK, Cooney TF, Nicol M (1992) High-temperature Raman investigation of order-disorder behavior in the $MgAl_2O_4$ spinel. Phys Rev B 45:500–502. https://doi.org/10.1103/PhysRevB.45.500

D'lppolito V, Andreozzi GB, Bersani D, Lottici PP (2015) Raman fingerprint of chromate, aluminate and ferrite spinels. J Raman Spectrosc 46:1255–1264. https://doi.org/10.1002/jrs.4764

DeAngelis BA, Keramidas VG, White WB (1971) Vibrational spectra of spinels with 1:1 ordering on tetrahedral sites. J Solid State Chem 3(3):358–363. https://doi.org/10.1016/0022-4596(71)90071-5

Droop GTR (1987) A general equation for estimating Fe^{3+} concentrations in ferromagnesian silicates and oxides from microprobe analyses, using stoichiometric criteria. Mineral Mag 51:431–435. https://doi.org/10.1180/minmag.1987.051.361.10

Dubessy J, Caumon MC, Rull F (2012) Raman spectroscopy applied to earth sciences and cultural heritage. EMU notes in mineralogy 12. https://doi.org/10.1180/EMU-notes.12

Errandonea D (2014) AB2O4 compounds at high pressures. In: Manjón FJ et al (eds) Pressure-induced phase transitions in AB2X4 chalcogenide compounds. Springer series in materials science 189. Springer-Verlag, Berlin Heidelberg, p 53–73. https://doi.org/10.1007/978-3-642-40367-5_2

Grimes NW, Collett AJ (1971) Correlation of infrared spectra with structural distortions in the spinel series Mg $(Cr_xAl_{2-x})O_4$. Phys Status Solidi B 43:591 – 599. https://doi.org/10.1002/pssb.2220430218

Gupta HC, Sood G, Parashar A, Tripathi BB (1989) Long wavelength optical lattice vibrations in mixed chalcogenide spinels $Zn_{1-x}Cd_xCr_2S_4$ and $CdCr_2(S_{1-x}Se_x)_4$. J Phys Chem Solids 50(9):925–929. https://doi.org/10.1016/0022-3697(89)90042-5

Keramidas VG, DeAngelis BA, White WB (1975) Vibrational spectra of spinels with cation ordering on the octahedral sites. J Solid State Chem 15(3):233–245. https://doi.org/10.1016/0022-4596(75)90208-X

Kharbish S (2010) Geochemistry and magmatic setting of Wadi ElMarkh island arc gabbrodiorite suite, central Eastern Desert, Egypt. Chem Erde-Geochem 70:257–266. https://doi.org/10.1016/j.chemer.2009.12.007

Kharbish S (2012) Raman spectra of minerals containing interconnected As(Sb)O_3 pyramids: trippkeite and schafarzikite. J Geosci-Czech 57:51–60. https://doi.org/10.3190/jgeosci.111

Kharbish S (2013) Metamorphism and geochemical aspects on Neoproterozoic serpentinites hosted chrome spinel from Gabal Al-Degheimi, Eastern Desert, Egypt. Carpath J Earth Environ 8(4):125–138. http://www.ubm.ro/sites/CJEES/viewTopic.php?topicId=379

Kharbish S (2016) Micro-Raman spectroscopic investigations of extremely scarce Pb-As sulfosalt minerals: baumhauerite, dufrénoysite, gratonite, sartorite and seligmannite. J Raman Spectrosc 47:1360–1366. https://doi.org/10.1002/jrs.4973

Kharbish S (2017) Spectral-structural characteristics of the extremely scarce silver arsenic sulfosalts, proustite, smithite, trechmannite and xanthoconite: μ-Raman spectroscopy evidence. Spectrochim Acta A 177:104–110. https://doi.org/10.1016/j.saa.2017.01.038

Kharbish S, Andráš P (2014) Investigations of the Fe sulfosalts berthierite, garavellite, arsenopyrite and gudmundite by Raman spectroscopy. Mineral Mag 78(5):1287–1299. https://doi.org/10.1180/minmag.2014.078.5.13

Kharbish S, Jeleň S (2016) Raman spectroscopy of the Pb-Sb sulfosalts minerals: boulangerite, jamesonite, robinsonite and zinkenite. Vib Spectrosc 85:157–166. https://doi.org/10.1016/j.vibspec.2016.04.016

Kharbish S, Andráš P, Luptáková J, Milovská S (2014) Raman spectra of oriented and non-oriented Cu hydroxy-phosphate minerals: libethenite, cornetite, pseudomalachite, reichenbachite and ludjibaite. Spectrochim Acta A 130:152–163. https://doi.org/10.1016/j.saa.2014.01.144

Laguna-Bercero MA, Sanjuán ML, Merino RI (2007) Raman spectroscopic study of cation disorder in poly- and single crystals of the nickel aluminate spinel. J Phys Condens Matter 19:1–10. https://doi.org/10.1088/0953-8984/19/18/186217

Lazzeri M, Thilbaudeau P (2006) Ab initio Raman spectrum of the normal and disordered $MgAl_2O_4$ spinel. Phys Rev B 74:140301-1–140301-4. https://doi.org/10.1103/PhysRevB.74.140301

Lenaz D, Lughi V (2013) Raman study of $MgCr_2O_4$–$Fe^{2+}Cr_2O_4$ and $MgCr_2O_4$–$MgFe_2^{3+}O_4$ synthetic series: the effects of Fe^{2+} and Fe^{3+} on Raman shifts. Phys Chem Miner 40:491–498. https://doi.org/10.1007/s00269-013-0586-4

Lenaz D, Lughi V (2017) Raman spectroscopy and the inversion degree of natural Cr-bearing spinels. Am Mineral 102:327–332. https://doi.org/10.2138/am-2017-5814

Lenaz D, Princivalle F (2005) Crystal chemistry of detrital chromian spinel from the southeastern Alps and outer Dinarides: the discrimination of supplies from areas of similar tectonic setting? Can Mineral 43(4):1305–1314. https://doi.org/10.2113/gscanmin.43.4.1305

Lenaz D, Skogby H (2013) Structural changes in the $FeAl_2O_4$ -$FeCr_2O_4$ solid solution series and their consequences on natural Cr-bearing spinels. Phys Chem Miner 40:587–595. https://doi.org/10.1007/s00269-013-0595-3

Libowitzky E (1999) Correlation of O-H stretching frequencies and O-H…O hydrogen bond lengths in minerals. Monatsh Chem 130(8):1047–1059. https://doi.org/10.1007/BF03354882

Malézieux JM (1985) Contribution a l'etude de spinelles de synthèse et de chromites naturelles par microsonde Raman laser. Dissertation, L'Universite des Sciences et Techniques de Lille. http://ori-nuxeo.univ-lille1.fr/nuxeo/site/esupversions/3a84faf8-9517-4559-a616-638678f6ab83

Malézieux JM, Barbillat J, Cervelle B, Coutures JP, Couzi M, Piriou B (1983) Étude de spineless de synthèse de la série $Mg(Cr_xAl_{2-x})O_4$ et de chromites naturelles par microsonde Raman-laser. Tschermaks Mineral Petrogr 32:171–185. https://doi.org/10.1007/BF01081108

Marinković Stanojević ZV, Romčević N, Stojanović B (2007) Spectroscopic study of spinel $ZnCr_2O_4$ obtained from mechanically activated ZnO–Cr_2O_3 mixtures. J Eur Ceram Soc 27:903–907. https://doi.org/10.1016/j.jeurceramsoc.2006.04.057

O'Neill HSTC, Dollase WA (1994) Crystal structures and cation distributions in simple spinels from powder XRD structural refinements: $MgCr_2O_4$, $ZnCr_2O_4$, Fe_3O_4 and the temperature dependence of the cation distribution in $ZnAl_2O_4$. Phys Chem Miner 20:541–555. https://doi.org/10.1007/BF00211850

O'Neill HSTC, Annersten H, Virgo D (1992) The temperature dependence of the cation distribution in magnesioferrite ($MgFe_2O_4$) from powder XRD structural refinements and Mössbauer spectroscopy. Am Mineral 77:725–740. http://www.minsocam.org/ammin/AM77/AM77_725.pdf

Park BH, Kim DS (1992) Thermodynamic properties of $NiCr_2O_4$–$NiFe_2O_4$ spinel solid solution. Thermochim Acta 205(17):289–298. https://doi.org/10.1016/0040-6031(92)85271-V

Preudhomme J, Tarte P (1971) Infrared studies of spinels III. The normal II-III spinels. Spectrochim Acta A 27:1817–1835. https://doi.org/10.1016/0584-8539(71)80235-0

Reddy BJ, Frost RL (2005) Spectroscopic characterization of chromite from the Moa-Baracoa ophiolitic massif, Cuba. Spectrochim Acta A 61:1721–1728. https://doi.org/10.1016/j.saa.2004.07.002

Redfern SAT, Harrison RJ, O'Neill HSTC, Wood DRR (1999) Thermodynamics and kinetics of cation ordering in $MgAl_2O_4$ spinel up to 1600 °C from in situ neutron diffraction. Am Mineral 84:299–310. http://www.AmMin/TOC/Articles_Free/1999/Redfern_p299-310_99.pdf

Shannon RD (1976) Revised effective ionic radii and systematic studies of interatomic distances in hallides and chalcogenides. Acta Crystallogr A 32(5):751–767. https://doi.org/10.1107/S0567739476001551

Sickafus KE, Wills JM, Grimes NW (1999) Structure of spinel. J Am Ceram Soc 82(12):3279–3292. https://doi.org/10.1111/j.1151-2916.1999.tb02241.x/abstract

Sinha MM (1999) Vibrational analysis of optical phonons in mixed chromite spinels. Nucl Instrum Methods B 153:183–185. https://doi.org/10.1016/S0168-583X(98)00994-X

Smith E, Dent G (2005) Modern Raman spectroscopy—a practical approach. Wiley, England. https://doi.org/10.1002/0470011831

Van Minh N, Yang IS (2004) A Raman study of cation-disorder transition temperature of natural $MgAl_2O_4$ spinel. Vib Spectrosc 35:93–96. https://doi.org/10.1016/j.vibspec.2003.12.013

Wang A, Jolliff BL, Haskin LA, 1999. Raman spectroscopic characterization of a Martian SNC meteorite: Zagami. J Geophys Res 104:8509 – 8519. https://doi.org/10.1029/1999JE900004

Wang A, Haskin LA, Kuebler KE, Jolliff BL, Walsh MM (2001) Raman spectroscopic detection of graphitic carbon of biogenic parentage in an ancient South African chert. Abstract No. 1423, Lunar Planetary Sci XXXII. http://www.lpi.usra.edu/meetings/lpsc2001/pdf/1423.pdf

Wang Z, Lazor P, Saxena SK, O'Neill HSTC (2002a) High pressure Raman spectroscopy of ferrite $MgFe_2O_4$. Mater Res Bull 37:1589–1602. https://doi.org/10.1016/S0025-5408(02)00819-X

Wang Z, O'Neill HSTC, Lazor P, Saxena SK (2002b) High pressure Raman spectroscopic study of spinel $MgCr_2O_4$. J

Phys Chem Solids 63:2057–2061. https://doi.org/10.1016/S0022-3697(02)00194-4

Wang A, Kuebler KE, Jolliff BL, Haskin LA (2004) Raman spectroscopy of Fe-Ti-Cr-oxides, case study: Martian meteorite EETA79001. Am Mineral 89:665–680. https://doi.org/10.2138/am-2004-5-601

White SN (2009) Laser Raman spectroscopy as a technique for identification of seafloor hydrothermal and cold seep minerals. Chem Geol 3–4:240–252. https://doi.org/10.1016/j.chemgeo.2008.11.008

Yong W, Botis S, Shieh SR, Shi W, Withers AC (2012) Pressure-induced phase transition study of magnesiochromite (MgCr2O4) by Raman spectroscopy and X-ray diffraction. Phys Earth Planet In 196–197:75–82. https://doi.org/10.1016/j.pepi.2012.02.011

Zhang ZW, Gan FX (2011) Analysis of the chromite inclusions found in nephrite minerals obtained from different deposits using SEM-EDS and LRS. J Raman Spectrosc 42:1808–1811. https://doi.org/10.1002/jrs.2963